A damage model for fretting contact between a sphere and a half space using semi-analytical method

Thibault Beyer, Thibaut Chaise, Julien Leroux, Daniel Nelias

A damage model for fretting contact between a sphere and a half space using semi-analytical method

Thibault BEYER[a,b], Thibaut CHAISE[a], Julien LEROUX[b], Daniel NELIAS[1a]

[a] *Univ Lyon,INSA-Lyon,CNRS UMR5259,LaMCoS,F-69621,France*
[b] *Safran Aircraft Engines, Centre de Villaroche, 77550 Moissy Cramayel, FRANCE*

Abstract

This paper presents a fast method of solving 3D contact problems when one of the mating bodies has an elastic-damageable behavior. The damage model is implemented in a semi-analytical model using Eshelby' s equivalent inclusion method in the contact solver. The proposed technique can be seen as an enrichment technique for which the effect of heterogeneous inclusions is surimposed on the homogeneous solution in the contact algorithm. Contact pressure and subsurface stress field computation time is kept small due to a massive use of 3D and 2D Fast Fourier Transforms. Cuboidal inclusions with the same size as the discretization of the half-space and with the same elastic properties are surimposed. The damage model affects the elastic properties of the cuboidal inclusions. The emphasis is put on the effects of the fretting regimes on the contact pressure and damage evolution.

Keywords: Contact Mechanics, Semi-Analytical Methods (SAM), Damage Mechanics, Fretting, Eshelby's Equivalent Inclusion Method (EIM), Inhomogeneity, Eigenstrain

1. Introduction

Fretting occurs when two body in contact are submitted to oscillatory tangential loading.

[1] corresponding author, daniel.nelias@insa-lyon.fr

Based on the amount of stick and slip that occurs in the contact two fretting sliding conditions can be differentiated : the partial slip condition and the gross slip condition [1]. For a circular contact in partial slip condition, the center of the contact is stick and a slip annulus appears at the edge of the contact [2] but in gross slip conditions all the contact surface is slipping.

Under fretting loading, cracks and surface degradation are appearing as a result of fatigue phenomenon, void nucleation and sub-surface crack propagation [3] [4]. Bryggman [5] explained the appearance of crack in partial slip conditions by the cyclic shearing of material in the contact region and, in the same way, wear would be caused by the propagation and intersections of these cracks.

Zhou and Vincent [6] have established three fretting regimes based on experimental results : the partial slip regime, the gross slip regime and the mixed fretting regime which corresponds to sliding conditions evolving from gross slip to partial slip due to a modification of the contact conditions. Wear is generally associated with the gross slip regime while the partial slip regime to cracks [7]. Both damage phenomenon compete on the mixed regime and material response fretting map associated with fretting regimes map has been proposed in [8].

Continuum Damage Mechanics (CDM) has been widely used to study failure due to fatigue [9]. Recently, CDM has been applied to study the damage phenomenons leading to wear and cracks initiation in material during fretting cycles [10, 11, 12, 13] and rolling/sliding contacts [14].

Raje et al. [15, 16] developed a damage model for rolling contact fatigue in which the material microstructure is modeled using Voronoi tessellation. The same model was used to study fretting fatigue [17] and fretting wear [18, 19]. Shen et al. [20] coupled an elastic-plastic damage model with wear in order to simulate fretting fatigue life. Kumar et al. [21] proposed a finite element simulation of fretting fatigue and studied the effects of the presence of voids inside the material. Finite element (FE) models have been developed by many authors for fretting [22] and wear computations [23, 24]. Recently, Yue et al. [25] proposed a finite element model of fretting wear with a variable coefficient of friction. But for three-dimensional problems and a moving load, a very fine

mesh is required for the contact interfaces and the computation costs become very high.

A numerical technique to simulate three-dimensionnal fretting has been investigated by Nelias and co-workers [26, 27, 28, 29] based on the semi-analytical method (SAM) initially proposed by Jacq et al. [30]. SAMs have been continuously developed and applied to several problems such as thermo-elasto-plastic contact modeling [31], modeling plasticity and accumulation of plastic strains [31] [32], running-in [33], simulation of single impact [34], shot peening [35] and low plasticity burnishing [36] [33] [37], modeling of cuboidal inclusions [38] [39] [40] [41], ellipsoidal inclusions [42, 43] [44], heterogeneous viscoelastic behavior [45] [46], heterogeneous elastoplastic behavior [47], as well as to account for material or coating anisotropy [48] [49].

The purpose of the present work is to use the damage mechanics approach to model the phenomenon leading to wear and cracks initiation in semi analytical methods. The proposed enrichment technique is using multiple damageable cuboidal inclusions surimposed on the homogeneous solution in the contact algorithm. The damage algorithm only affects the Young's modulus of the inclusions and, by this way, modifies the contact solution. Fretting simulation have been performed in both gross slip and partial slip conditions The emphasis is put on the effects of the fretting regimes on the contact pressure and damage evolution.

2. Theoretical Background and model description

2.1. Contact problem formulation

Generally, the formulation of the contact between two finite bodies (Fig. 1) consists in a set of equations and inequalities that are recalled below:

- The load balance : the applied load W and the integration of the contact pressure $p(x, y)$ in the contact region Γ_c must be strictly equal.

$$W = \int_{\Gamma_c} p(x, y) d\Gamma \tag{1}$$

- The surface separation : the gap between the two contacting surfaces is:

$$h(x,y) = h_i(x,y) + \delta + u_z^{(B_1+B_2)}(x,y) \tag{2}$$

where $h_i(x,y)$ is the initial geometry, δ the rigid body displacement, and $u_z^{(B_1+B_2)}(x,y)$ the sum of normal displacements of surfaces 1 and 2, that can be due to elastic deflection (under loading only), plastic deformation or the presence of inhomogeneities.

- The contact conditions : the distance $h(x,y)$ is always positive, because the contacting bodies can not interpenetrate each other. The conditions are defined by the inequalities:

$$h(x,y) \geqslant 0$$

$$\text{contact} : h_i(x,y) = 0 \text{ and } p(x,y) > 0$$

$$\text{separation} : h_i(x,y) > 0 \text{ and } p(x,y) = 0 \tag{3}$$

- The tangential contact conditions can be written using the Coulomb's friction law to express the shear stresses q_τ in the contact. The tangential load Q and the contact zone Γ_c are known from the solution of the normal problem. The following system of equation needs to be solved to determine the sticking region Γ_{st} and the slipping region Γ_{sl}.

$$q_\tau(x,y) = -\mu \cdot p(x,y) \cdot \frac{\Delta s_\tau(x,y)}{\parallel \Delta s_\tau(x,y) \parallel} \qquad \forall (x,y) \in \Gamma_{sl} \tag{4}$$

$$\Delta u_\tau(x,y) - \Delta \delta_\tau = \Delta s_\tau(x,y) \qquad \forall (x,y) \in \Gamma_{sl} \tag{5}$$

$$\parallel q_\tau(x,y) \parallel < \mu \cdot p(x,y) \qquad \forall (x,y) \in \Gamma_{st} \tag{6}$$

$$\Delta u_\tau(x,y) - \Delta \delta_\tau = 0 \qquad \forall (x,y) \in \Gamma_{st} \tag{7}$$

$$\sum_{\Gamma_p} q(x,y) S = Q \tag{8}$$

$$\Gamma_{sl} \cup \Gamma_{st} = \Gamma_c \tag{9}$$

δ_τ is the tangential rigid body displacement and s_τ is the relative slip amplitude. The tangential surface displacement u_τ is the result of the displacements coming from both the shear stresses and the normal pressure field.

These equations are solved simultaneously using the Conjugate Gradient Method (CGM) as proposed by Polonsky and Keer [50].

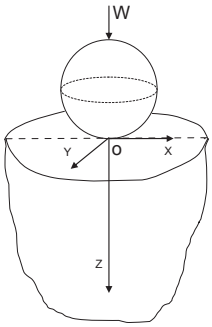

Figure 1: Contact of rigid indenter over a elastic half-space.

2.2. Eshelby's equivalent inclusion method in Contact Mechanics

The presence of a single or multiple inhomogeneities within one of the bodies in contact is taken into account by adding in Eq. (2) the eigendisplacement u_z^* induced by these inhomogeneities. Equation 2 is then modified as follows:

$$h(x,y) = h_i(x,y) + \delta + u_z(x,y) + u_z^*(x,y) \tag{10}$$

The bases of the method in the case of an elastic or elastic-plastic half-space are detailed extensively in [42, 43, 44, 47].

Sections 2.2.2 and 2.2.3 present the various steps for the calculation of u_z^* in the case of an elastic body containing elastic inhomogeneities. First, the calculation of the eigenstrain ε^* is presented followed by the calculation of the subsurface stresses and finally the calculation of the eigendisplacement u_z^* is detailed.

2.2.1. Eshelby's solution for an infinite space

An infinite matrix M with the elastic stiffness tensor C^M_{ijkl} containing an ellipsoidal domain Ω with the elastic stiffness tensor C^I_{ijkl} is submitted at infinity to a uniform strain ε^0. The strain field is disturbed by the presence of the inhomogeneity.

The Eshelby's equivalent inclusion method (EIM) consists in representing the ellipsoidal inhomogeneity as an inclusion having the same elastic propreties C^M_{ijkl} as the matrix but being subjected to an additional imaginary strain called eigenstrain ε^* giving:

$$C^I_{ijkl}(\varepsilon^0_{kl} + \varepsilon_{kl}) = C^M_{ijkl}(\varepsilon^0_{kl} + \varepsilon_{kl} - \varepsilon^*_{kl}) \quad \text{in } \Omega \tag{11}$$

The necessary and sufficient condition for the equivalence of the stresses and strains in the two above problems of inhomogeneity and inclusion is provided by Eq. (11). In particular, the eigenstrain ε^*_{ij} is related to compatibility strain ε_{ij} by:

$$\varepsilon_{ij} = S_{ijkl} \times \varepsilon^*_{kl}, \tag{12}$$

where S_{ijkl} is the Eshelby's tensor. Substitution of Eq. (12) into Eq. (11) leads to:

$$\Delta C_{ijkl} S_{klmn} \varepsilon^*_{mn} + C^M_{ijkl} \varepsilon^*_{kl} = -\Delta C_{ijkl} \varepsilon^0_{kl} \tag{13}$$

where

$$\Delta C_{ijkl} = C^I_{ijkl} - C^M_{ijkl}$$

Moschovidis and Mura [51] extended Eshelby's solution to two close ellipsoidal inhomogeneities. In recent work, multiple inclusions problems have been solved by using a conjugate gradient algorithm to determine each unknown eigenstrain [39, 40, 42].

2.2.2. Half-space solution

Three dimensional contact problems involve a half-space that is bounded by the surface plane $z = 0$ in the cartesian coordinate system (x, y, z) as shown in Fig. 1. Jacq et al. [30] and later Zhou et al. [38] proposed a method allowing

to extend previous solution, valid only for infinite spaces, to half spaces. The solution for an isotropic half space consists in decomposing the problem into three subproblemes (Fig. 2), known as Chiu's decomposition [52].

(1) An inclusion with the prescribed eigenstrain $\varepsilon^* = (\varepsilon^*_{xx}; \varepsilon^*_{yy}; \varepsilon^*_{zz}; \varepsilon^*_{xy}; \varepsilon^*_{xz}; \varepsilon^*_{yz})$ in an infinite space.

(2) A symmetric inclusion with a mirror eigenstrain $\varepsilon^*_s = (\varepsilon^*_{xx}; \varepsilon^*_{yy}; \varepsilon^*_{zz}; \varepsilon^*_{xy}; -\varepsilon^*_{xz}; -\varepsilon^*_{yz})$ in the same space.

(3) A normal traction distribution $-\sigma^n$ at the surface of the half space $(z = 0)$ which is a function of the eigenstrains ε^* and ε^*_s.

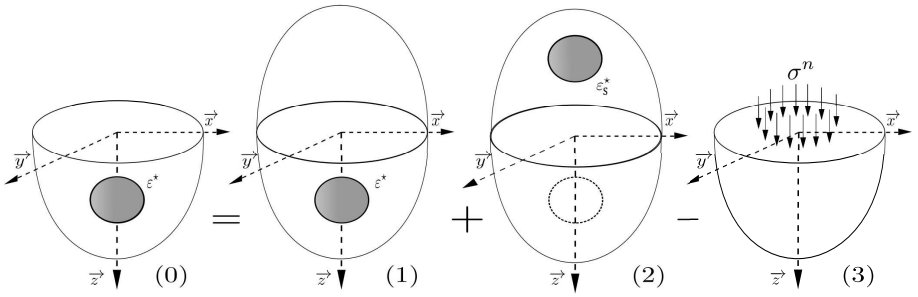

Figure 2: Decomposition of the half-space solution into three sub-problems.

The summation of the two solutions (1) and (2) leaves the plane of symmetry $(z = 0)$ free of shear tractions. By adding an opposite normal stress σ^n, the condition of free surface traction is obtained. The stress at any point of the domain meshed with $n_x \times n_y \times n_z$ cuboids is given by:

$$\begin{aligned}\sigma_{ij}(x,y,z) = &\sum_{x^I=0}^{n_x-1}\sum_{y^I=0}^{n_y-1}\sum_{z^I=0}^{n_z-1} B_{ijkl}(x-x^I, y-y^I, z-z^I)\varepsilon^*_{kl}(x^I,y^I,z^I) \\ &+ \sum_{z^I=0}^{n_z-1}\sum_{y^I=0}^{n_y-1}\sum_{x^I=0}^{n_x-1} B_{ijkl}(x-x^I, y-y^I, z+z^I)\varepsilon^*_{skl}(x^I,y^I,-z^I) \\ &- \sum_{y^I=0}^{n_y-1}\sum_{x^I=0}^{n_x-1} M_{ij}(x-x^I, y-y^I, z)\sigma^n(x^I,y^I,0)\end{aligned} \tag{14}$$

where B_{ijkl} are the influence coefficients that relate the constant eigenstrain

at the point (x^I, y^I, z^I) which is the inclusion center in an infinite space to the stress σ_{ij} at the point (x, y, z). M_{ij} represent the influence coefficients relating the normal traction σ^n within a discretized area centered at $(x^I, y^I, 0)$ to the stress σ_{ij} at the point (x, y, z).

$$B_{ijkl}(x) = C^M_{ijmn} D_{mnkl}(x) \quad \text{for } x \text{ in } D - \Omega \tag{15}$$

$$B_{ijkl}(x) = C^M_{ijmn} (D_{mnkl}(x) - I_{mnkl}) \quad \text{for } x \text{ in } \Omega \tag{16}$$

where $I_{ijkl} = \frac{1}{2} (\delta_{il}\delta jk + \delta_{ik}\delta jl)$ is the fourth-order identity tensor.

The expression for D_{ijkl} is given in Mura [53].

$$D_{ijkl} = \frac{1}{8\pi(1-\nu)} [\Psi_{,ijkl} - 2\nu\delta_{kl}\phi_{,ij} - (1-\nu)(\delta_{kl}\phi_{il} + \delta_{ki}\phi_{,jl} + \delta_{jl}\phi_{,ik} + \delta_{li}\phi_{,jk})] \tag{17}$$

$$\Psi(x) = \int_\Omega |x - x'| dx'$$
$$\phi(x) = \int_\Omega \frac{1}{|x - x'|} dx'$$

For a single inclusion centered at (x^I, y^I, z^I) in the half-space, the normal traction σ^n at the surface point $(x^{'}, y^{'}, 0)$ is obtained as:

$$\begin{aligned} \sigma^n(x', y', 0) = &- B_{33kl}(x' - x^I, y' - y^I, -z^I,)\varepsilon^*_{kl}(x^I, y^I, z^I) \\ &- B_{33kl}(x' - x^I, y' - y^I, z^I,)\varepsilon^*_{skl}(x^I, y^I, -z^I) \end{aligned} \tag{18}$$

In Eq. (14), each component $M_{ij}()$ is obtained by a double integration of the function $F_{ij}()$ over a discretized surface area $2\Delta x \times 2\Delta y$ centered at $(x^I, y^I, 0)$, see appendices A and B.

$$M_{ij}(x - x^I, y - y^I, z) = \int_{x^I - \Delta x}^{x^I + \Delta x} \int_{y^I - \Delta y}^{y^I + \Delta y} F_{ij}(x - x', y - y', z) dx' y' \tag{19}$$

The 3D-FFT is used to accelerate the calculation of the first (1) and second terms (2) and the 2D-FFT for the third term (3). Wrap around order and zero-padding techniques are used in order to remove the induced periodicity error [54].

2.2.3. Normal displacement of a surface point

The surface normal 'eigen-displacements' can be obtained when inserting the eigenstrain into the total strain. They are generated by the pressure field σ^n only. The normal displacements are calculated as:

$$u_z^*(x,y) = \sum_{y'=0}^{n_y-1} \sum_{x'=0}^{n_x-1} K^n(x-x', y-y')\sigma^n(x', y') \tag{20}$$

To solve the equation above numerically, the surface in contact is discretized into $n_1 \times n_2$ rectangular elements of uniform size $2\Delta x \times 2\Delta y$. Then, pressure and displacement within each discrete patch are treated as constant and their values located at the center. The effect of a uniform pressure on a rectangular area has been given by Love [55] and Johnson [56]. K^n denotes the influence coefficients that relate the normal pressure at the surface point $(x', y', 0)$ to the normal displacement at the surface point $(x, y, 0)$, recalled in Appendix C.

2.2.4. Integration of the inhomogeneity effects in the contact algorithm

In order to integrate the inhomogeneity effects in the contact algorithm, an equivalent elastic algorithm is proposed. The effect of an inclusion on the contact problem derives from the fact that the surface contact geometry is modified by the eigen-displacement produces by the eigenstrain. The contact pressure and shears are then updated, which modifies the eigenstrain value. The elastic displacements are obtained from the updated contact pressure via the resolution of the elastic contact problem. The algorithm is repeated until convergence of the normal displacements is obtained. The equilibrium between the contact problem and subsurface problem is checked at every time step of the loading cycle.

2.3. Damage model

In the elastic heterogeneous contact solver presented in 2.2.4, a Continuum Damage Mechanics (CDM) based model was implemented in order to describe the degradation of material due to contact loading. During fretting cycles, the

high contact stresses are causing micro-cracks in the material responsible of wear or fatigue cracks [7, 3, 4, 5]. Sections 2.3.1 and 2.3.2 present the basics of continuum damage mechanic and his application when coupled with elasticity. Sections 2.3.3 highlights the implementation of the damage model in the heterogeneous contact algorithm.

2.3.1. Continuum Damage Mechanics

Continuum Damage Mechanics (CDM) background permits to describe the initiation and evolution of degradation in materials at the microscale such as micro cracks and voids. The damage model used in the current approach is isotropic and based on a single scalar damage variable D introduced by Kachanov [57]). Considering no healing of the material, D is monotonically increasing from $D = 0$, the undamaged state, to $D = 1$ the complete local rupture of the material.

The state of stress in the damaged material can be described by the effective stress introduced by Rabotnov [58]:

$$\tilde{\sigma} = \frac{\sigma}{(1 - D)} \tag{21}$$

Following Lemaitre [59] strain equivalence hypothesis, the strain behavior is modified by damage only through the effective stress. Hence, the strain associated with a damaged state under the applied stress is equivalent to the strain associated with its undamaged state under the effective stress. Applying the Hooke's law with E, the modulus of elasticity for the undamaged material, the elastic strain in the damaged material becomes:

$$\varepsilon = \frac{\tilde{\sigma}}{E} = \frac{\sigma}{(1 - D)E} \tag{22}$$

From this equation it can be deduced that an increase in the damage manifests as the reduction in the modulus of elasticity as shown in Fig. 3. D characterizes the effect of microscopic phenomenon on the macroscopic behavior of the material as a strength loss. These usually reproduce the presence of micro-cracks within an elastic material.

2.3.2. Elasticity Coupled with Damage

In order to model the damage of concretes, predominant in tension ,Mazars [60] used the scalar damage parameter D coupled with elasticity in his 3D model. Mazars [60] choosed D as a function of the positive (tensile) strains and to evaluate these strains, he defined the following scalar called equivalent strain:

$$\tilde{\varepsilon} = \sqrt{\sum_{i=1,3} \langle \varepsilon_i \rangle_+^2} \tag{23}$$

with

$$\langle \varepsilon_i \rangle_+ = \left(\frac{\varepsilon_i + |\varepsilon_i|}{2} \right) \tag{24}$$

and ε_i the principal strains. However, to study the damage of contact under fretting, D needs to take into account tensile, compressive and shear stresses.

An adaptation of the expression of Mazars's equivalent strain is proposed here :

$$\tilde{\varepsilon} = \sqrt{\sum_{i=1,3} \langle \varepsilon_i \rangle_+^2 + \sum_{i=1,3} \langle \varepsilon_i \rangle_-^2} = \sqrt{\sum_{i=1,3} \varepsilon_i^2} \tag{25}$$

with

$$\langle \varepsilon_i \rangle_- = \begin{cases} |\varepsilon_i| \quad if \quad \varepsilon_i \leq 0 \\ 0 \quad if \quad \varepsilon_i > 0 \end{cases} \tag{26}$$

The equivalent strain is now traducing the local three-dimensional state of deformation of the solid via a uniaxial scalar variable.

The equivalent strain controls the growth of the damage variable according to an evolving threshold. At the end of every time step and for every point of the discretization of the half-space, the loading function can be defined as :

$$f(\varepsilon, D) = \tilde{\varepsilon} - K(D) \tag{27}$$

$K(D)$ takes the largest value of the equivalent strain $\tilde{\varepsilon}$ ever reached by the material during the loading history at the considered point. $K(D = 0)$ is initialized at ε_{d0}, the damage threshold strain, corresponding to the strain at

the elastic limit.

$$\begin{cases} K(D) = \varepsilon_{d0} \quad if \quad D = 0 \\ K(D) = \max_t \tilde{\varepsilon} \qquad if \quad D \geq 0 \end{cases} \tag{28}$$

If the threshold is reached, a new increment of damage called δD is added to the damage variable at the considered point. The evolution law for the damage variable is defined as:

$$\begin{cases} \delta D = \dfrac{\tilde{\varepsilon} - K(D)}{\varepsilon_R - \varepsilon_{d0}} \quad if \quad \tilde{\varepsilon} \geq K(D) \\ \qquad\qquad\qquad\qquad\qquad\qquad \rightarrow D = D + \delta D \\ \delta D = 0 \qquad if \quad \tilde{\varepsilon} < K(D) \end{cases} \tag{29}$$

with ε_R the strain leading to a macroscopic cracks.

The behavior of the material is linear elastic on the first part of Fig. 3. When the equivalent strain reaches the damage threshold, the local elastic properties of the matrix are modified through the presence of micro-cracks which decreases the strength of the material. This local decrease of the modulus of elasticity is irreversible.s From ε_{d0}, the damage threshold strain, the damage variable will modified the elastic behavior of the material by decreasing the Young's modulus as illustrated in Fig. 3 and until the material strain reaches the macroscopic fracture strain ε_R (see Fig. 4b).The damage evolution is always increasing and locally linear by pieces (Fig. 4a).

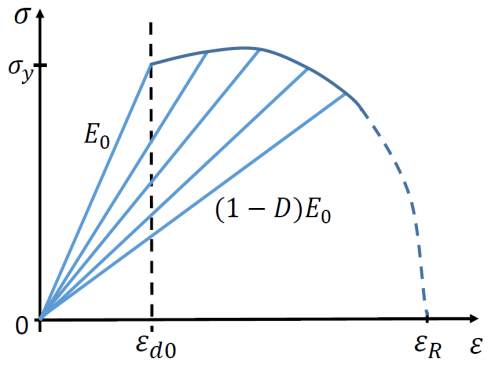

Figure 3: Stress-Strain plot with damage evolution.

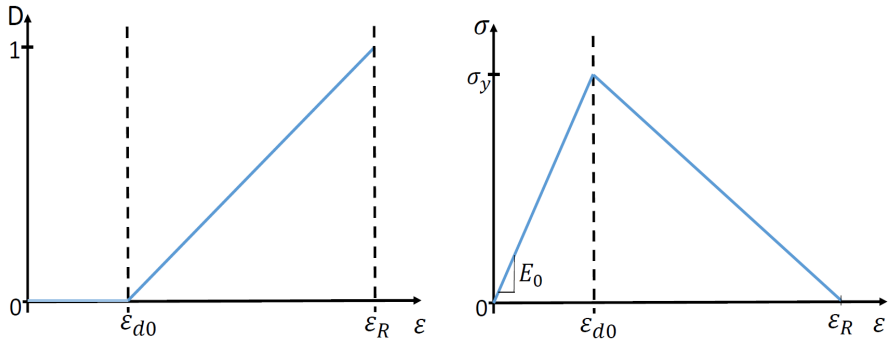

(a) (b)

Figure 4: (a) Damage evolution as a function of strain showing the purely elastic domain and the damageable domain. (b) Purely elastic and damageable domain on a stress strain plot.

2.3.3. Integration of the damage model in the contact algorithm

The damage model defined in 2.3.2 is coupled with the semi-analytical contact solver developed by Nelias and co-workers [28, 43]. This method is based on the solution developed by Love [55] for a rectangular patch of pressure over a homogeneous half space. The Eshelby's equivalent inclusion method is used as an enrichment technique in order to introduce a local modification of the Young's modulus of the material. Multiple cuboidal inclusions with the same size as the discretization of the half-space and initially with the same elastic properties are surimposed on the half-space as presented in Fig. 5. The effect of damage on the material is traduced through the modification of the Young's modulus of the inclusions. Leroux et al.[42] and Koumi et al.[44] have shown that the contact pressure distribution may be significantly modified by the presence of inhomogeneities close to the surface, which subsequently affect the subsurface stress distribution. The Young's modulus of the inclusions are modified by the damage variable D and hence affect the contact pressure distribution through the contribution of eingenstrains. One of the main advantage of the method is to compute only the stress field in the area around the contact (at the surface but also in depth). It has been observed that damage usually happened just

under the contact during fretting [5]. For sake of computational efficiency, the half-space has been enriched only in this area. Note that no damage occurs far from the contact. When the first element is reaching a damage value equal to 1, the simulation is stopped. It should be noted that in CDM, $D = 1$ means that the element is too damaged to ensure continuity which can lead to the initiation of crack. In order to continue the simulation once an element damage value reaches 1, the contact surface should be modified by removing the element. Depending of the area concerned and of the localization of the damage, it can be interpreted as wear or crack initiation. It should be noted that because simulations are stopped when a first element damage value reaches 1, the present model is only simulating the phenomena leading to the first appearance of wear or crack.

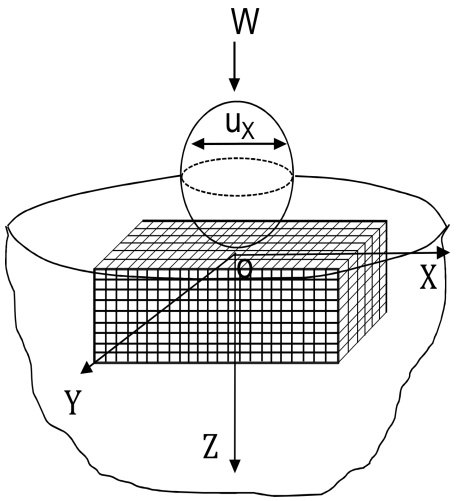

Figure 5: 3D view of a sphere on a elastic half-space with multiple cuboidal inclusions surimposition.

The main step of the algorithm, sumerized on the flowchart in Fig. 6 are described here :

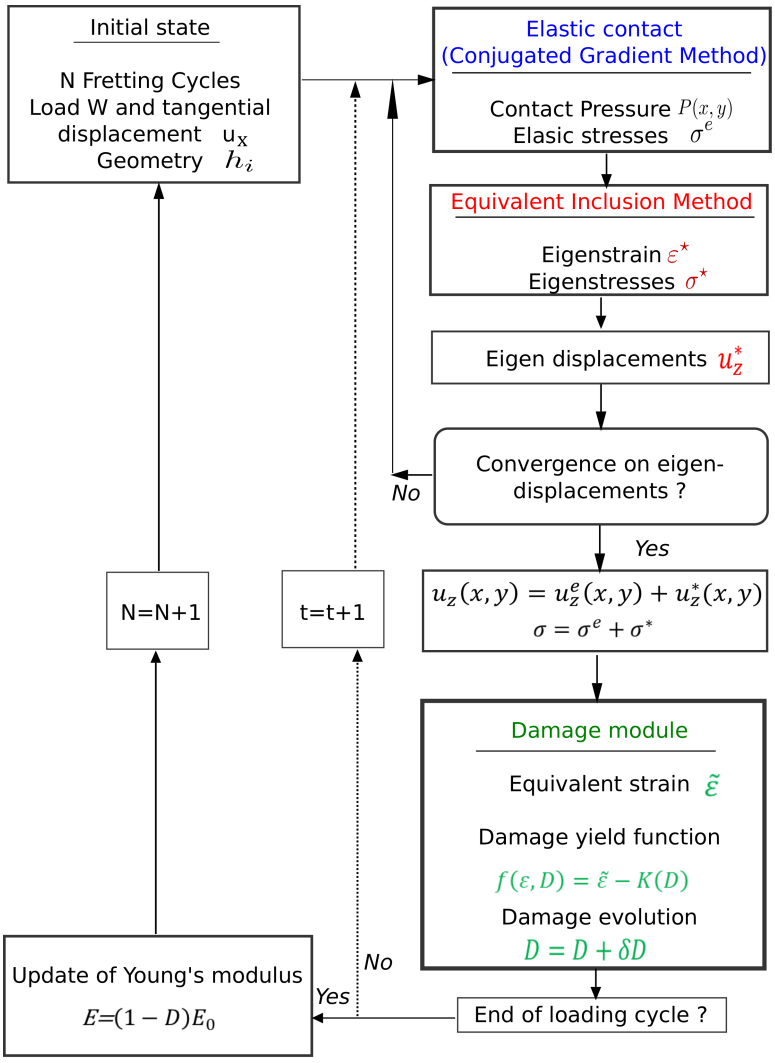

Figure 6: Algorithm of Heterogeneous Elastic-Damageable Contact Problem

1^{st} Fretting Cycle :

- **Step1**:

  Solve the elastic contact problem for the initial loading increment, and determine the elastic stresses and strains in the solid.

- **Step2**: Damage module

  Compute the equivalent strains for the current loading increment.

Test the damage criterion for each inclusion and determine the inclusion's damage increments δD for the current time step.
Increment the loading and solve the elastic problem again.
Compute the equivalent strains and, after testing the damage criterion, determine the inclusion's damage increment δD.
Repeat until the last loading increment of the loading cycle.

- **Step3**: At the end of the cycle:
  Update the corresponding Young's modulus with the damage variable computed during the loading cycle.

I^{th} **Fretting Cycle :**

- Assign to each inclusion the new Young's modulus.

- Repeat the previous steps for the considered loading cycle. Compute elastic stresses, equivalent strains and the damage increments δD for every time step of the cycle.

- At the end of the fretting cycle, if one-or more-of inclusions are totally damaged : stop the calculation.

3. Validation

For validation purpose of the enrichment technique, a comparison with the analytical Hertzian solution is performed. Note that the heterogeneous semi-analytical method has been compared and validated in previous work with both analytical solutions [42] and finite element simulation [44]. A 3D rigid sphere in contact with a heterogeneous half-space has been simulated with the semi-analytical method. The half-space Young's modulus and Poisson's ration are

choosen as $E_0 = 210$GPa and $\mu_0 = 0.3$, respectively. The normal applied load is $W = 410$N. For the homogeneous half-space, this load leads to a contact radius $a^* = 0.32$mm and a maximum contact pressure $P_0 = 1890.8$MPa. The half-space is discretized in $67 \times 67 \times 51$ computation points such as the space between the constituted is $2\Delta x = 2\Delta y = 2\Delta z = 0.062a^*$. Then the half-space is filled from the free surface to a defined thickness with cuboidal inclusions centered on computation points and having the same dimensions as the discretization. The enrichment is constituted of $N_x \times N_y \times N_z = 62 \times 62 \times 36$ cuboids as illustrated in Fig. 5.

A comparison between the analytical Hertzian contact solution and the contact solution founded with the enriched half-space is given for the pressure distribution, for the half space stresses along axis z and axis y at surface ($z = 0$) as shown in Fig. 7. A very good agreement is found which in turn validates the numerical enrichment technique.

4. Results

4.1. Description of the problem

In this section the contact simulation between a rigid sphere of radius R=25mm and a homogeneous half-space is presented. The contacting bodies are subjected to an oscillatory tangential motion. The two bodies are first brought into contact with a normal load $W = 410$N. A tangential displacement along the x direction is then applied. The half-space Young's modulus and Poisson's ration are choosen as $E_0 = 210$GPa and $\mu_0 = 0.3$, respectively. For the homogeneous half-space, this load leads to a Hertzian contact radius $a^* = 0.32$mm and a maximum contact pressure $P_0 = 1890.8$MPa. The imposed rigid body displacement is cycling between $u_x = 0.025$mm and $u_x = -0.025$mm ($u_x/a^* = 0.078$) to reproduce an entire fretting loop. The fretting cycle is decomposed into multiple time steps as shown in Fig. 8.

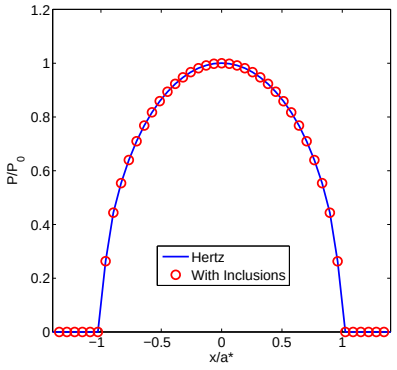

(a)

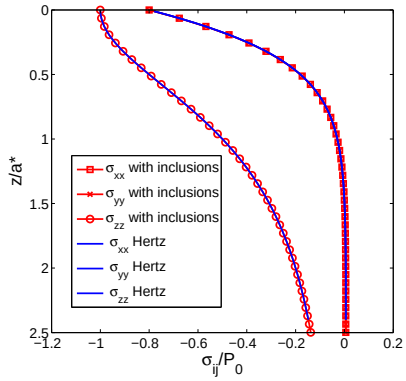

(b)

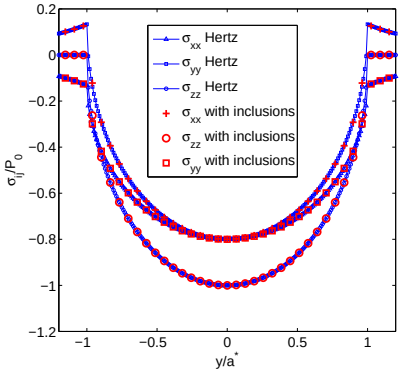

(c)

Figure 7: Validation of the enrichment technique with Hertzian analytical solution (a) Pressure distribution (b) Stresses along z direction (c) Stresses along y direction

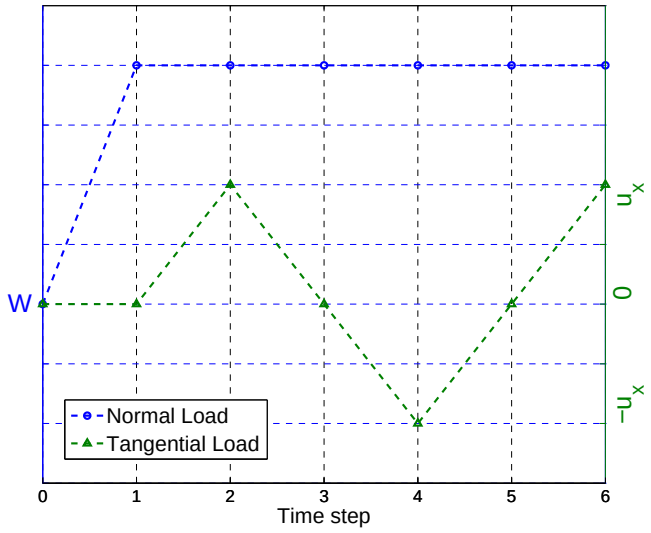

Figure 8: Normal and tangential load during one fretting cycle.

The half-space has been enriched with damageable elastic cuboidal inclusions with the same properties than the half-space. The damage model, as presented in section 2.3.2 is used with two parameters : $\varepsilon_R = 0.036$ and $\varepsilon_{d0} = 0.003225$. Firstly, results in the case of the gross slip regime are presented, afterwards the partial slip regime is investigated and finally, simulation in the case of coated materials are presented.

4.2. Simulation in gross slip regime

Here are presented the results of contact simulations in gross slip regime. According to Coulomb's law, the shear distribution is equal to the coefficient of friction times the pressure along the contact surface : $Q = \mu \times P$.

For unlubricated fretting, the coefficient of friction is generally high [61] and main phenomenon are wear and cracks. That's why all simulations have been performed with a friction coefficient $\mu \geq 0.3$.

A first fretting simulation is presented with a coefficient of friction $\mu = 0.5$. In Fig. 9, the distribution of the equivalent strain $\tilde{\varepsilon}$ is shown for normal and

tangential loading conditions for the undamaged material. It can be observed that the maximum value of $\tilde{\varepsilon}$ is reached at depth around $z/a^* = 0.5$ under the surface for a normal loading. When a tangential displacement is added, the maximum value of $\tilde{\varepsilon}$ is reached at the surface and is more than 50% higher than with normal load only. All damage simulations have been performed until at least one point reached the critical damage value $D = 1$. The distribution of the scalar damage variable D at the end of fretting simulation is plotted at the contact surface $z = 0$ and in the plane $x = 0$ in Fig. 10a and Fig. 10b. It can be observed that the maximum damage is located at the center of the contact surface where the contact pressure is the higher and where the surface has seen the biggest sliding amplitude.

Figure 11 represents the evolution of the damage variable and the associated Young's modulus for the most damaged point of the material during fretting cycles. As the Young's modulus is decreasing, the equivalent strain is increasing and the material is becoming more damaged until the damage variable reaches its critical value and the Young's modulus has dropped to 0.

As the damage variable increases, contact pressure decreases (Fig. 12) and consequently, the contact area increases to respect the load equilibrium (Eq. 1). Moreover, the contact pressure drops locally by almost 40% at the center of the contact, where the surface is the more damaged. These results are in good agreements with the numerical results obtained by Shen et al. [20].

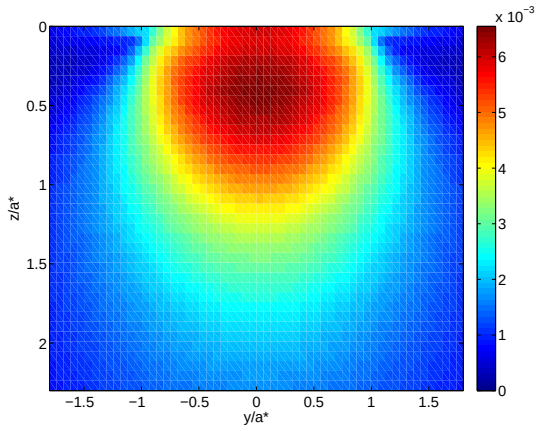

(a)

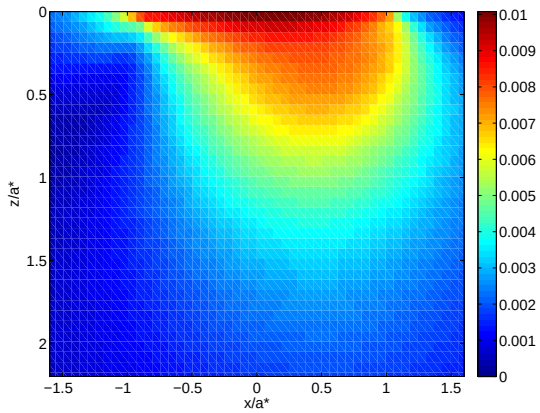

(b)

Figure 9: Equivalent strain $\tilde{\varepsilon}$ (a) under normal loading in the plane $x = 0$. (b) under normal and tangential loading in the plane $y = 0$ with $\mu = 0.5$ during the first fretting cycle.

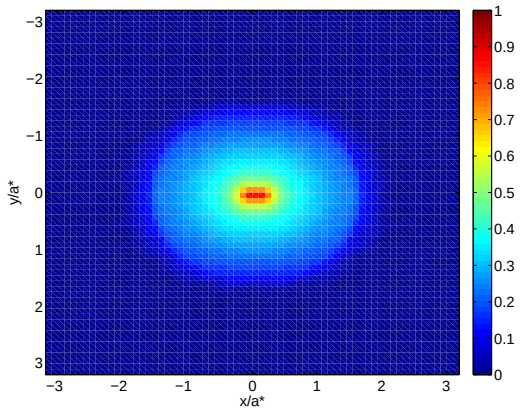

(a)

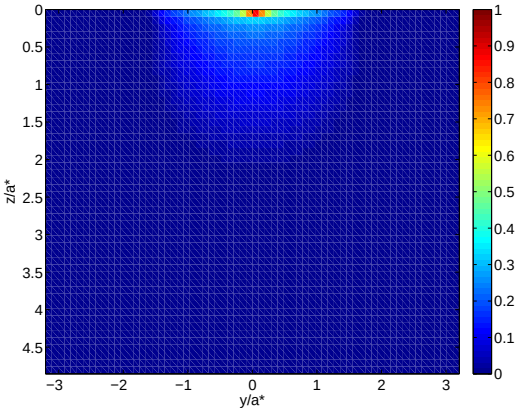

(b)

Figure 10: Damage variable D with $\mu = 0.5$ (a) in the plane $z = 0$. (b) in the plane $x = 0$ after 17 cycles.

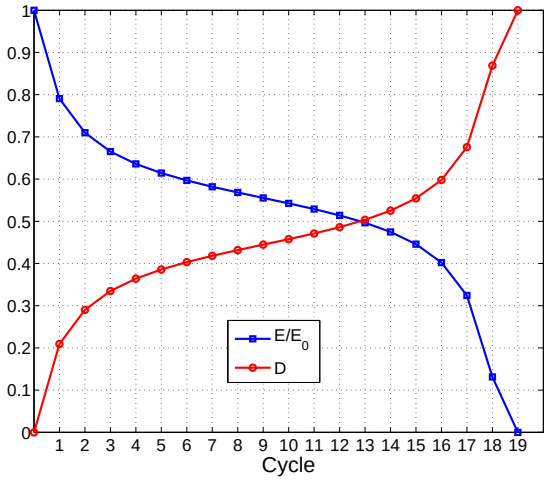

Figure 11: Evolution of damage and Young modulus with cycles for $\mu = 0.5$

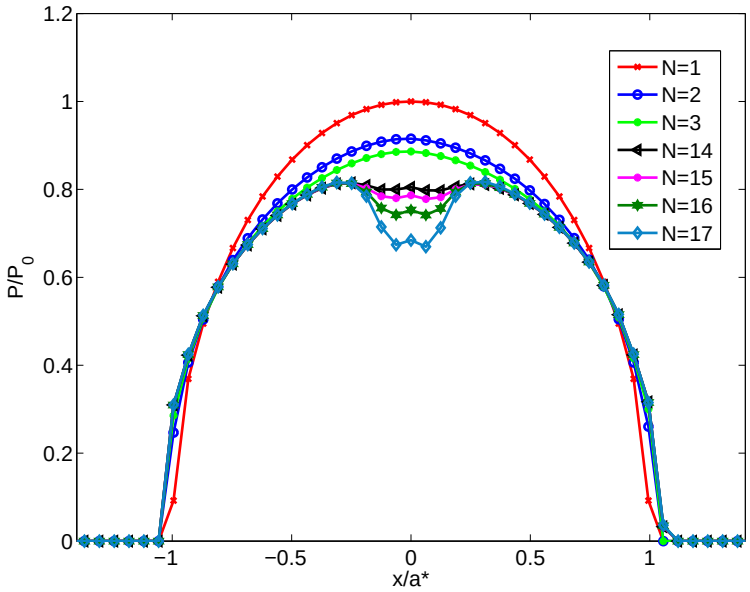

Figure 12: Effect of damage on contact pressure for $\mu = 0.5$

4.2.1. Effect of the coefficient of friction

Simulations were then performed in order to identify the influence of the friction coefficient on the model response. Firstly, values of the equivalent strain $\tilde{\varepsilon}$ along direction z for different coefficients of friction are compared in Fig. 13. It can be observed that for $\mu < 0.3$, the highest value of $\tilde{\varepsilon}$ is localized in the subsurface under the center of the contact while for $\mu \geq 0.3$, it is localized at the surface $z = 0$. Note that during unlubricated fretting conditions, the friction coefficient is usually high [61]. The following studies will focus on friction coefficient $\mu \geq 0.3$.

It can be observed in Fig. 16 that a higher coefficient of friction leads to an increased surface damage rate. It comes from the fact that, according to Coulomb's law, the higher is the coeffcient of friction, the higher are the surface shear stresses. That is why the damage surface is larger with $\mu = 0.7$ (Fig. 14a and Fig. 14b) than for $\mu = 0.5$ and the pressure distribution is dropping on a larger surface (see Fig. 15). It should be noted that the number of cycles leading to failure is significantly lower than what can be found in literature.

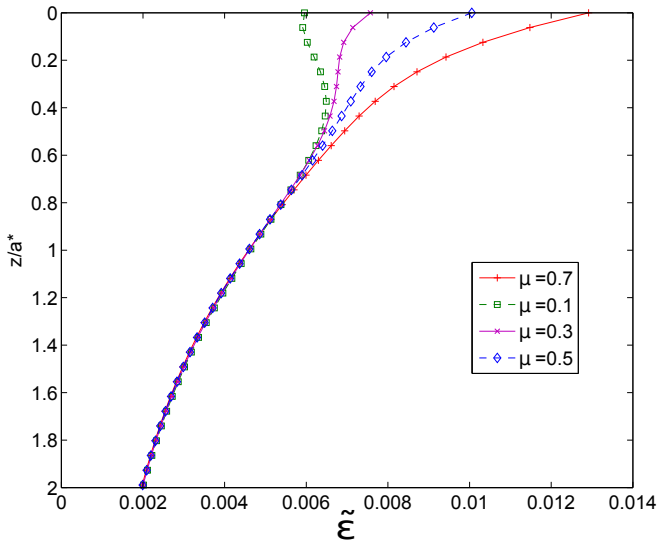

Figure 13: Equivalent strain $\tilde{\varepsilon}$ along direction z for different friction coefficients.

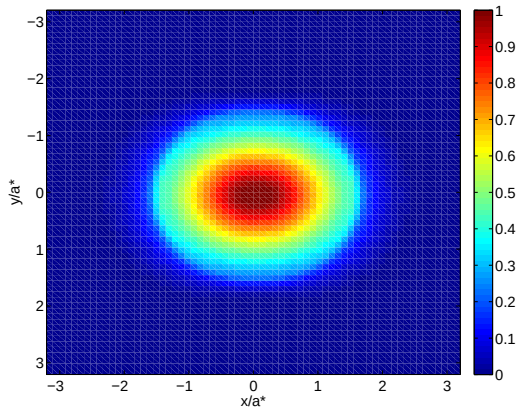

(a)

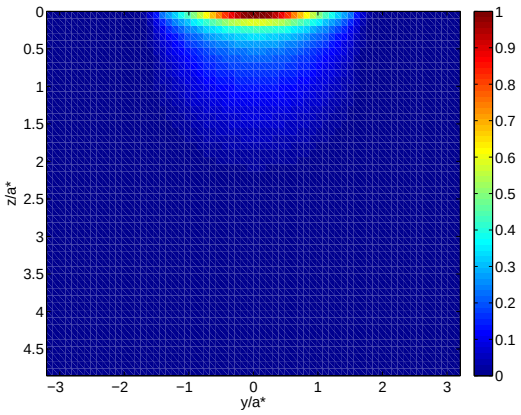

(b)

Figure 14: Damage variable D with $\mu = 0.7$ (a) in the plane $z = 0$. (b) in the plane $x = 0$ after 4 cycles.

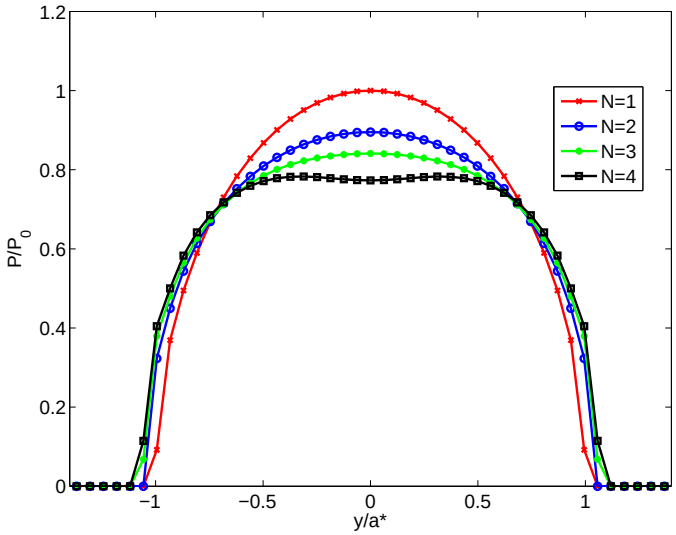

Figure 15: Effect of damage on contact pressure for $\mu = 0.7$

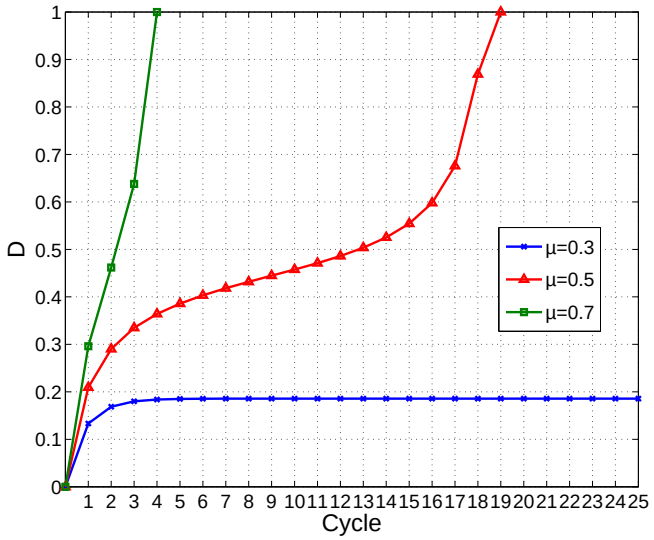

Figure 16: Evolution of damage function of friction coefficient

4.2.2. Effect of computation discretization on damage evolution

The reference space between the computation point is defined as $2\Delta x = 0.062a^*$ in section 3. Simulations are performed with different discretization sizes and the damage evolution of the most damage point is plotted in Fig. 17. There is no effect of the discretization size on the damage computation at the beginning of the simulation but after a few cycles, damage values are slowly diverging. For an identical damage value, different discretizations are modifying the Young's modulus in a different material volume. In the following cycles, the stress field will not be the same for the different discretizations.

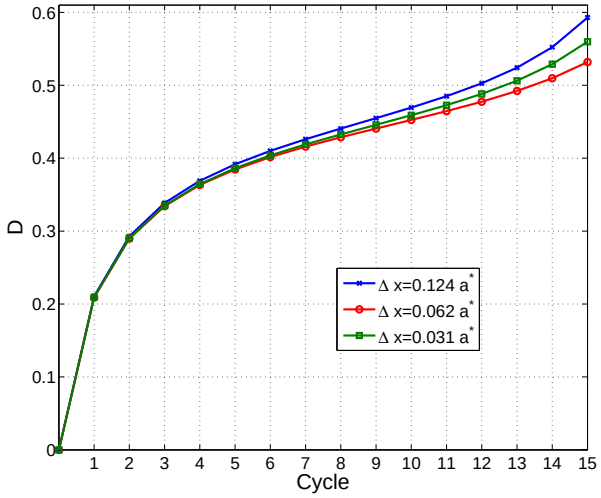

Figure 17: Evolution of damage function of enrichment width.

4.2.3. Effect of enrichment size on damage evolution

The half-space is constituted of $N_x \times N_y \times N_z$ cuboids as illustrated in Fig. 5. Fretting simulations are performed with $\mu = 0.5$ and with different enrichment sizes and plotted in Fig. 18. The enrichment depth $N_z = 2.23a^*$ is kept the same for every simulation. N_x and N_y are equals and vary from $2a^*$ to $4a^*$. One can observe that no effect of the size of the enrichment is observed on the damage evolution nor on contact pressure (see Fig. 19).

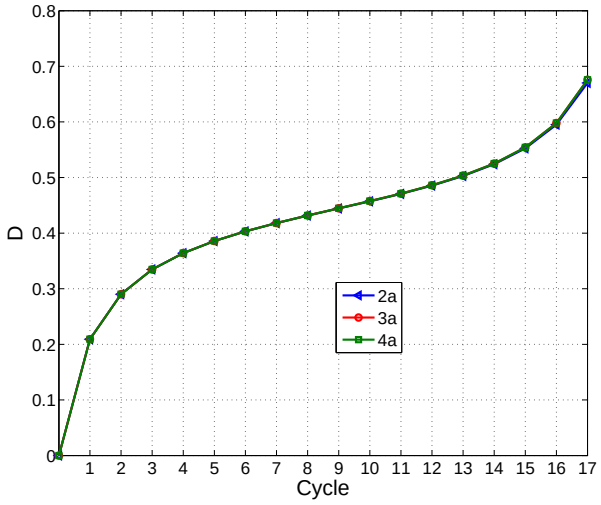

Figure 18: Evolution of damage function of enrichment width.

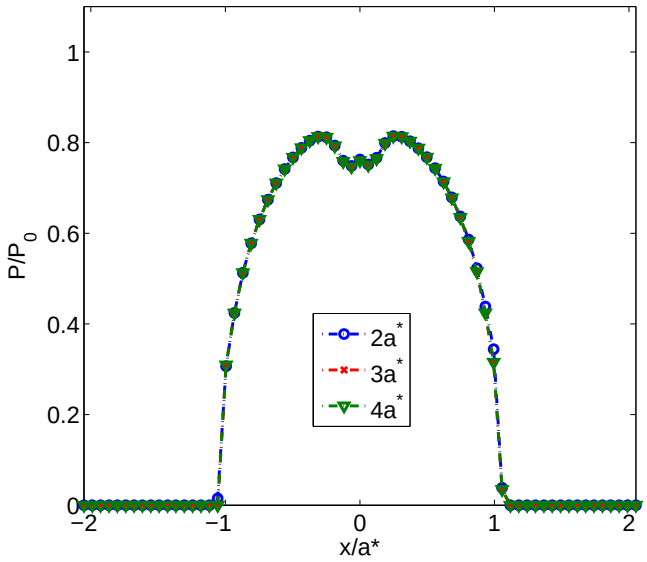

Figure 19: Comparison of contact pressure at the end of the damage simulation function of enrichment width.

4.3. Simulation in partial slip regime

In this section, the same damage model is used in the partial slip regime. A gross slip fretting loop is associated to wear whereas the partial slip regime is associated to cracking appearance. In partial slip regime the center of the contact is sticking and an annular slip zone is appearing at the edge of the contact area as shown in [2]. Acordingly to fretting material response fretting map, cracking appearance is generally associated whith smaller displacement amplitude and higher normal loading than in gross slip conditions [7].

A simulation is performed using a coefficient of friction of $\mu = 0.7$ and a normal load $W = 900$N. Accordingly with Hertzian theory, this load leads to a contact radius $a^* = 0.41817$mm and a maximum contact pressure $P_0 = 2457.386$MPa. The tangential displacement is imposed with a value of $u_x = 0.001$mm or $u_x/a^* = 0.0023$. The damage model parameters are kept the same as in section 4.1.

The state of the scalar damage variable D at the end of fretting simulation can be observed at the contact surface $z = 0$ and in the plane $x = 0$ in Fig. 20a and Fig. 20b after five fretting cycles. The higher damage values are localized in the slip circular zone at the edge of the contact. It is where the material sees the maximum strain during fretting cycles. In agreement to that, the pressure distribution is locally dropping at the contact edge as the damage is increasing (Fig. 21). During the damage progression, the contact area is increasing to respect the load equilibrium (Eq. 1) and the shear maximum value is moving out of the initial contact area (Fig. 22). These results exhibits the same effects of damage on contact pressure that the ones found in Ghosh et al. [18].

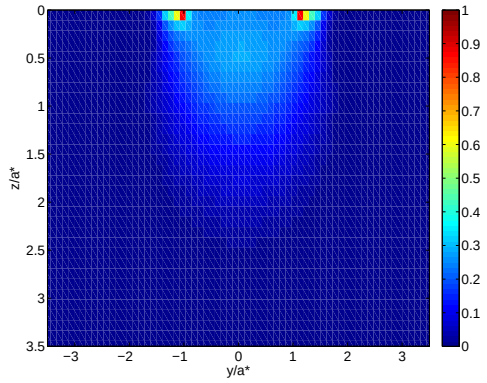

(a)

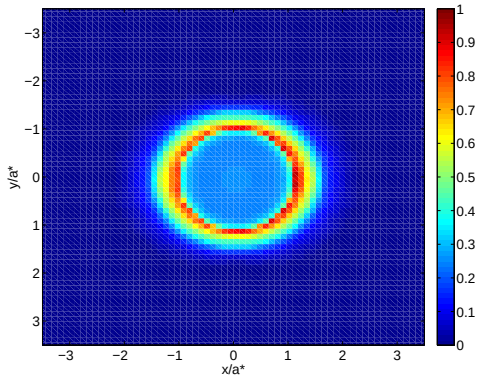

(b)

Figure 20: Damage variable D with $\mu = 0.7$ (a) in the plane $z = 0$. (b) in the plane $x = 0$ after 5 cycles.

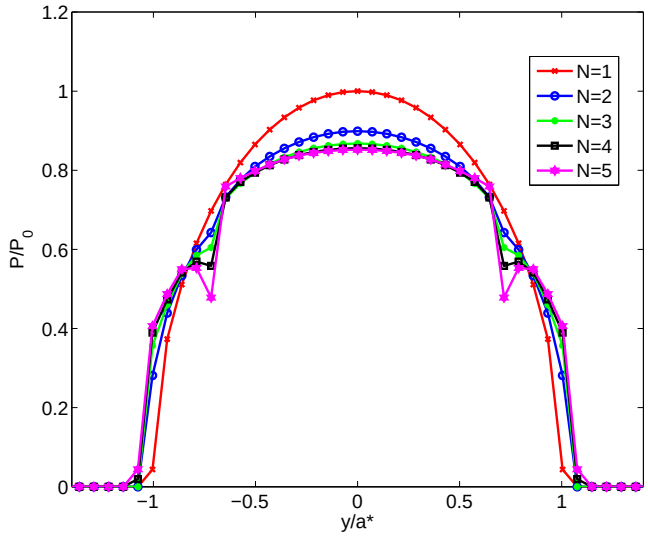

Figure 21: Evolution of contact pressure with damage in the plane x=0 for =0.7

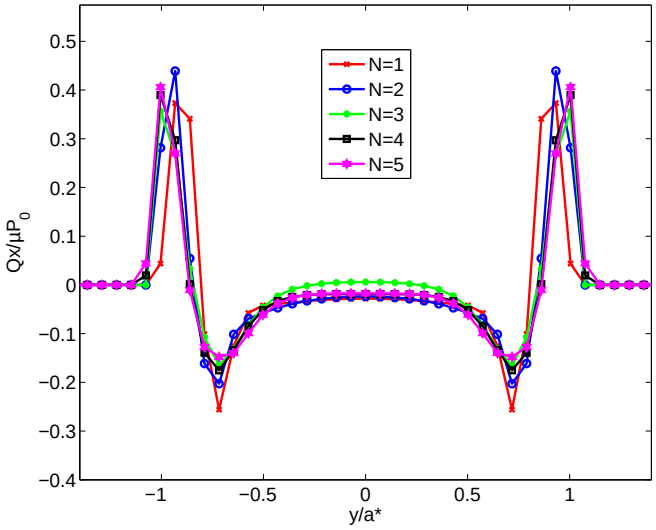

Figure 22: Evolution of contact shear distribution with damage in the plane x=0 for =0.7

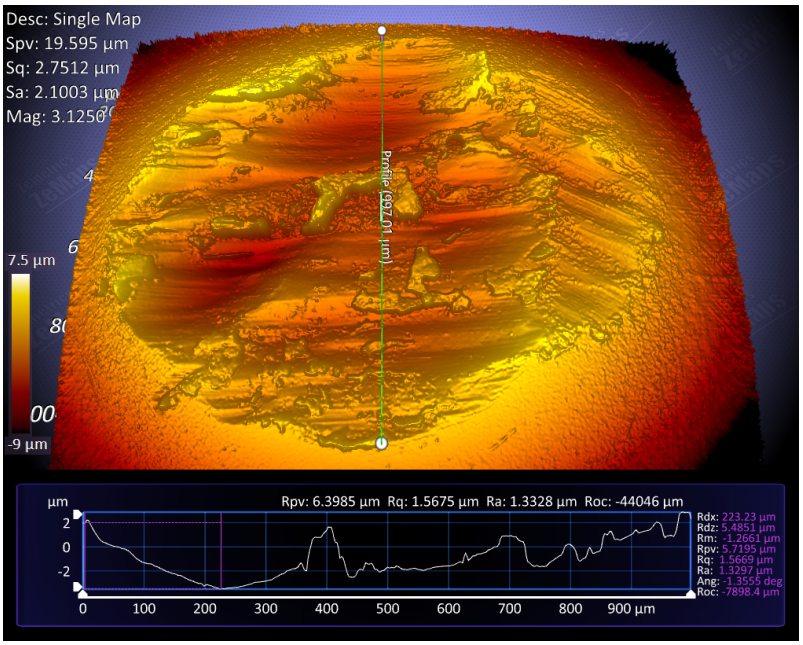

Figure 23: Wear scar of a steel ball under gross sliding

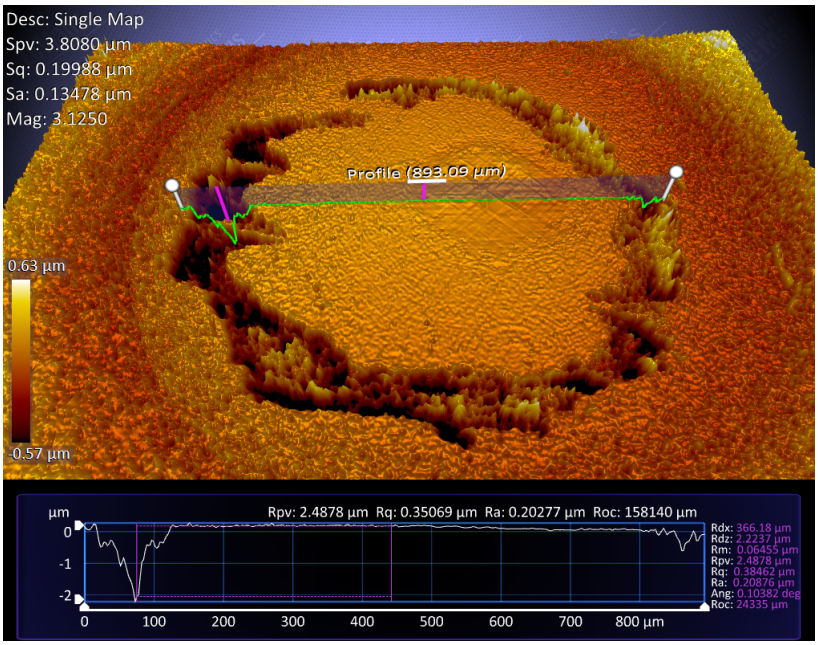

Figure 24: Wear scar of a steel ball under stick-slip

The results obtained in sections 4.2 and 4.3 are qualitatively in good agreement with the surface damage phenomenon usually observed in fretting conditions, see for example our experimental results in Figs. 23 and 24 – that can be compared to Figs. 14 and 20 – or to literature data [7].

4.4. Comparison with another damage model

In this section, the damage law used in Ghosh et al. [18] is presented and implemented into the semi-analytical contact solver. Fretting simulations are performed in gross slip regime and results are compared between the two damage models. A damage evolution law with an isotropic damage variable D based on the work of Chaboche and Lesne [62] is implemented and recalled here:

$$\frac{dD}{dN} = \frac{0.8 S_{ut}}{E} \frac{\Delta\tau}{H(1-D)} \tag{30}$$

with N the number of stress cycles, S_{ut} the ultimate tensile strength of the material, E the Young's modulus and H the hardness of the material. $\Delta\tau$ is the shear stress reversal at the considered point during a fretting cycle. Details leading to this equation can be found in Ghosh et al. [18].

The shear stress amplitude during one fretting cycle is calculated using the semi-analytical contact solver and damage evolution is calculated at every point of the material domain using Equation 30. For sake of computational efficiency, the number of cycles leading to the first fully damage element is computed using the jump-in-cycles algorithm proposed by Lemaitre [9] and already used in finite element simulation by Slack et al. [63]. This method assumes a linear damage evolution over a block of cycles.

4.4.1. Gross slip regime

Contact between a rigid sphere of radius $R = 25$mm and a homogeneous half-space is simulated using the semi-analytical solver. The same material and loading characteristics than in section 4.1 are used with a coefficient of friction $\mu = 0.7$.

The half-space has been enriched with damageable elastic cuboidal inclusions with initially the same properties than the half-space. The damage model proposed in Ghosh et al. [18] is used with two parameters: $S_{ut} = 2500$ MPa and $H = 1$ GPa. The damage increment used in the jump-in-cycles algorithm is chosen to be $\Delta D = 0.01$. All damage simulations have been performed until at least one point reached the critical damage value $D = 1$. Results in the case of gross slip regime and partial slip regime are investigated. The distribution of the scalar damage variable D at the end of fretting simulation is plotted at the contact surface $z = 0$ and in the plane $x = 0$ in Fig. 25. It can be observed that the maximum damage point is located at the center of the contact surface as observed with the previous model in Fig. 14. As the damage variable increases, contact pressure decreases (Fig. 26) and consequently, the contact area increases to respect the load equilibrium (see Eq. 1). Moreover, the contact pressure found at the last cycle with the two models are similar. A small difference is found between the two pressures due to the fact that simulation is stopped once the damage variable reaches the value $D = 1$ for the first time. The represented contact pressure is computed with the damage state from the previous cycle and depending on the damage evolution law, the damage level at this previous cycle is not exactly the same in the two models.

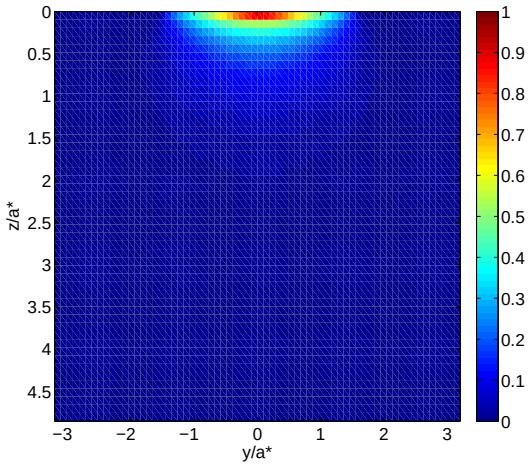

(a)

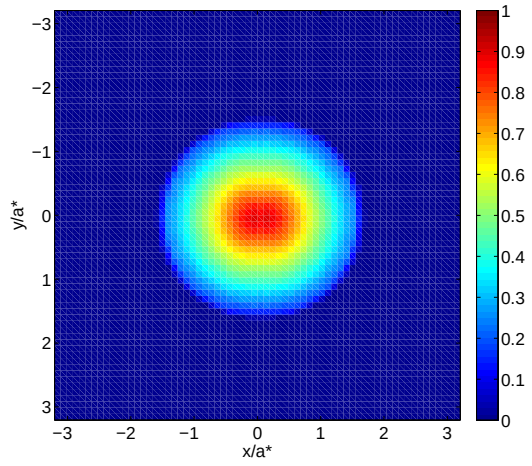

(b)

Figure 25: Damage variable D with $\mu = 0.7$ (a) in the plane $x = 0$. (a) in the plane $z = 0$ after 28 loading cycles using damage model from Ghosh et al. [18].

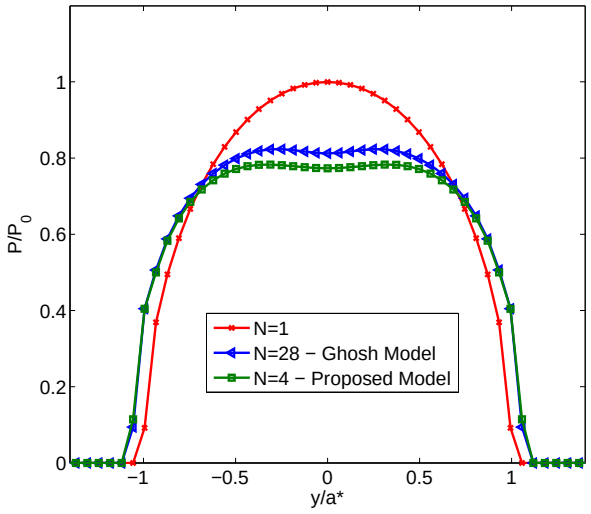

Figure 26: Contact pressure with damage in the plane x=0 for =0.7 at the last iteration of the simulation for the two models.

The number of damage cycles found in this damage model is equal to 28 compared to 4 in the proposed model. Therefore one damage cycle in our model is equivalent to approximately 7 cycles in the model of Ghosh et al. [18] in this specific example i.e. with the defined hardness and tensile strength.

4.5. Application to coated materials

A lot of materials used in the industry are coated to protect the surface from damage or to help keeping the integrity of the substrate. Hard metallic coatings can mitigate fretting by reducing friction and resisting crack initiation [64, 65]. Using the same enrichment technique as before gives the possibility to simulate coated materials. From the top surface until a defined thickness z_c cuboidal inclusions with different material properties than the substrate are used. Above this layer, the same material properties than the substrate are used for the inclusions (see Fig. 27).

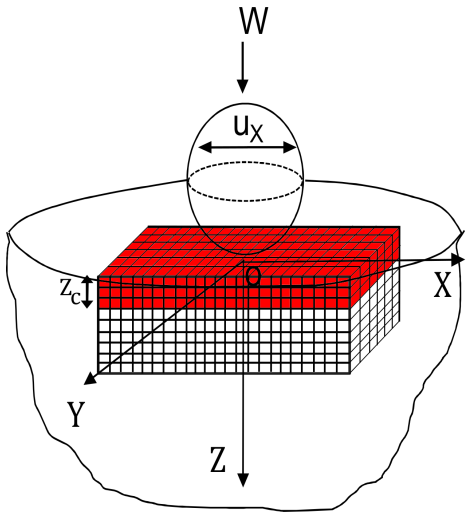

Figure 27: Enrichment of the half space with cuboidal inclusions to simulate the effect of coatings.

This section only aims to investigate the effects of elastic coatings on the localization of damage in the material. Firstly, only the distribution of equivalent strain $\tilde{\varepsilon}$ is studied. Different coating' s stiffnesses (with a Young modulus ratio defines as $\gamma = E/E_0$ with E and E_0 the modulus of the coating and substrate, respectively.) and thickness (z_c) are studied and the effect on damage evolution is analyzed. Two different coating stiffnesses are studied here, a harder one with $\gamma = 2$ and a softer one with $\gamma = 0.5$. The equivalent strain $\tilde{\varepsilon}$ is plotted in order to represent the coating effect on the damage localization. The same parameters as in section 4.1 are used for the contact loading.

In Figs. 28 and 29, the equivalent strain $\tilde{\varepsilon}$ is plotted for the undamaged material during the first cycle in the plane $y = 0$ for four different coating thicknesses z_c and for both coating stiffness ratios γ. These results are compared to the uncoated model along the axe z in Figs. 30 and 31.

For $\gamma = 0.5$, the maximum equivalent strain $\tilde{\varepsilon}$ is always located in the coated material (see Fig. 28) and $\tilde{\varepsilon}$ is very attenuated in the substrate. Moreover, the equivalent strain $\tilde{\varepsilon}$ in the coating is almost twice the value of $\tilde{\varepsilon}$ in the uncoated half-space (Fig. 30).

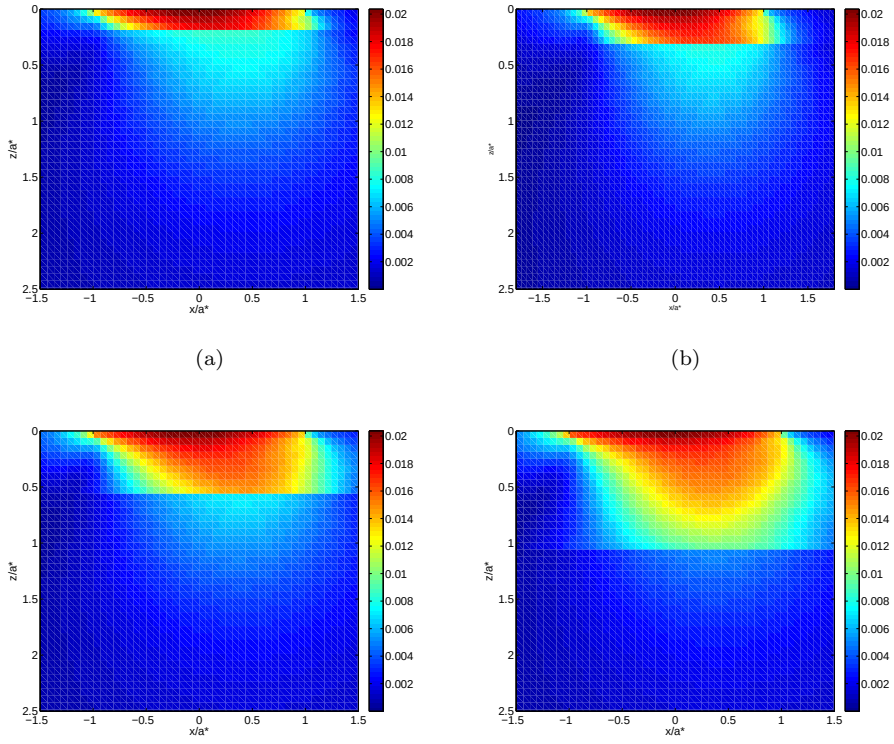

(a) (b)

(c) (d)

Figure 28: Equivalent strain $\tilde{\varepsilon}$ with a soft coating ($\gamma = 0.5$) of thickness (a) $z_c = 0.125a$ (b) $z_c = 0.25a$ (c) $z_c = 0.5a$ (d) $z_c = a$

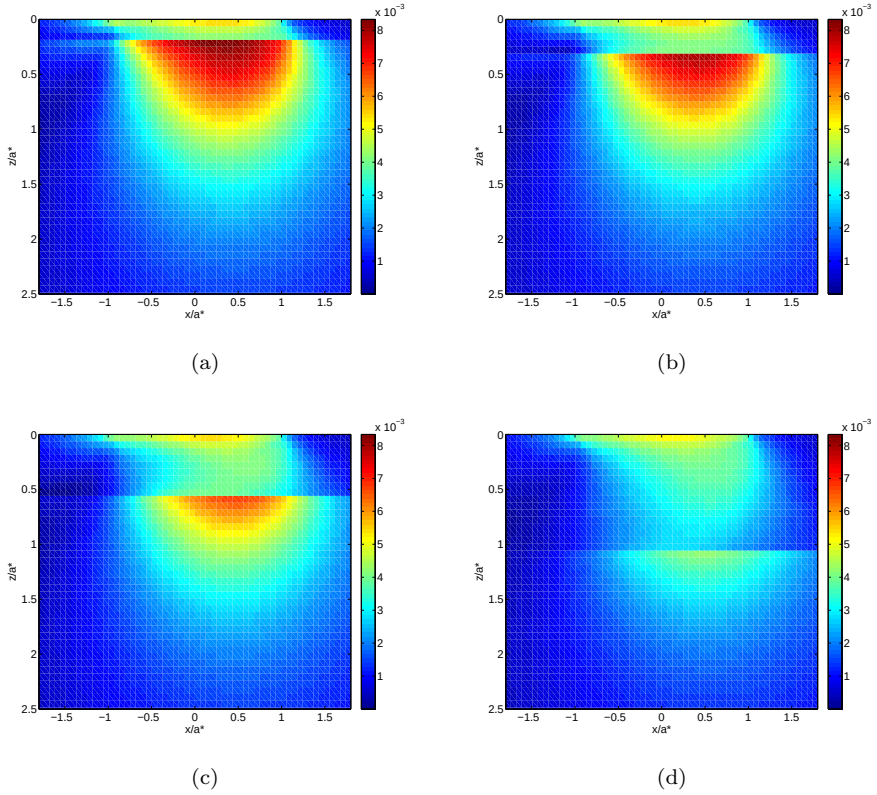

Figure 29: Equivalent strain $\tilde{\varepsilon}$ with a hard coating ($\gamma = 2$) of thickness (a) $z_c = 0.125a$ (b) $z_c = 0.25a$ (c) $z_c = 0.5a$ (d) $z_c = a$

In contrary to soft coatings, the maximum equivalent strain $\tilde{\varepsilon}$ is always located in the substrate material (see Fig. 29) for hard coatings ($\gamma = 2$). Moreover, the maximum equivalent strain $\tilde{\varepsilon}$ in the hard coating is almost two times lower than with the uncoated half space (Fig. 31). It is important to notice that the maximum of the equivalent strain $\tilde{\varepsilon}$ is located at the interface between the coating and the substrate for a coating thickness $z_c/a^* \approx 0.5$ (close to the maximum shear stress localisation). In the case of $z_c = a^*$, there is no high equivalent strain $\tilde{\varepsilon}$ at the interface. The layered structure of hard coatings leads to damage propagation at the interface between the coating and the substrate parallel to the surface as shown in [66].

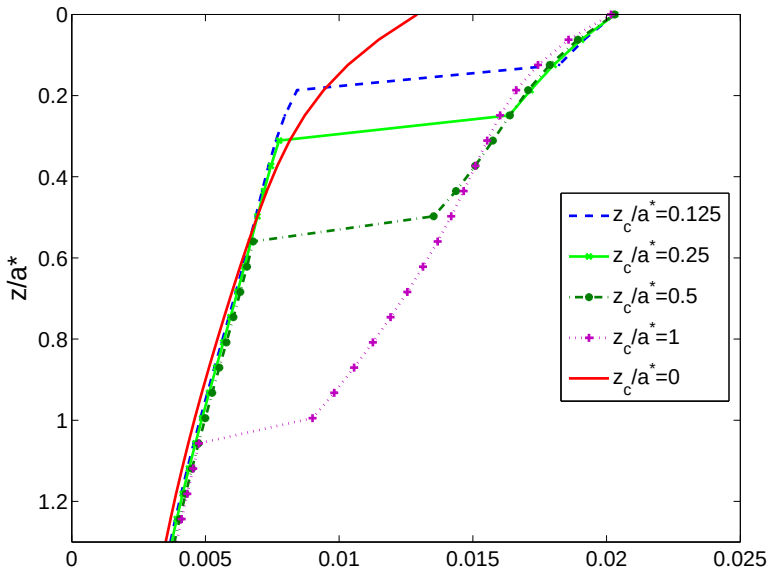

Figure 30: Equivalent strain along z for different thickness z_c and with a soft coating ($\gamma = 0.5$)

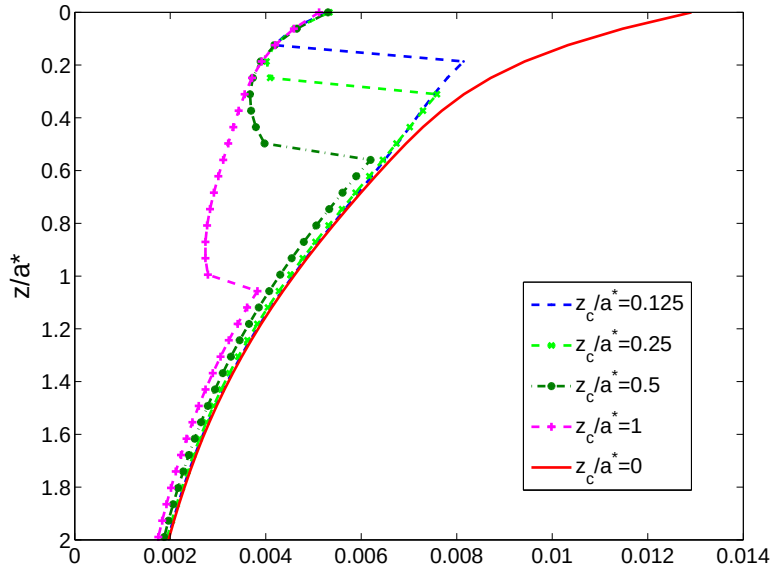

Figure 31: Equivalent strain along z for different thickness z_c and with a hard coating ($\gamma = 2$)

The damage variable D is plotted in Fig. 32, along the z-axis for the two different coating stiffnesses for a coating thickness $z_c = 0.25a$ after one fretting cycle. A strong hypothesis is made here that the damage parameters are the same for the coating and for the substrate even if there are not from the same material.

It can be observed that, accordingly with what was previously observed with $\tilde{\varepsilon}$, the soft coating is a lot more damaged than the hard one. Moreover, for the hard coating, the maximum damage is located at the interface between the substrate and the coating. But for the soft coating, the maximum of damage is located at the surface and is much higher (around 5 times).

The results presented here show that hard coatings are effective to protect the material from fretting surface degradations while soft coatings are damaging faster than uncoated material assuming that the damage threshold in term of yield strengh (ε_{d0}) and ductility (ε_R) are the same.

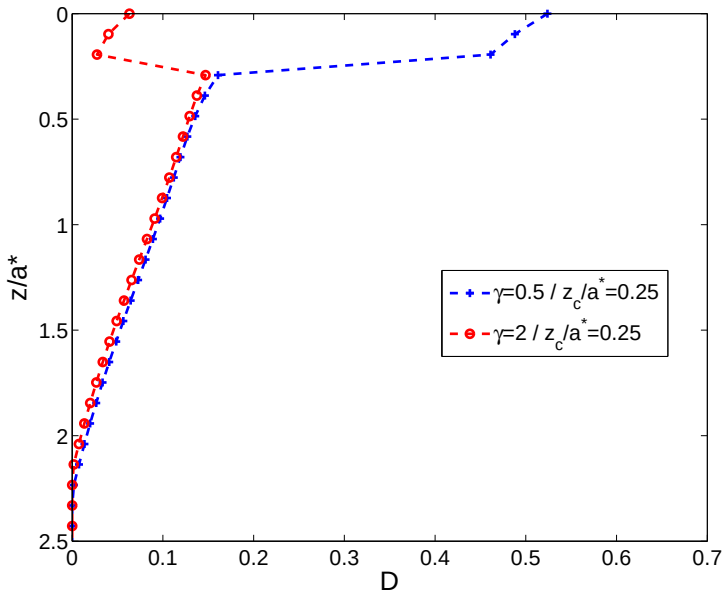

Figure 32: Damage after one fretting cycle along z direction for two different coating stiffnesses

5. Conclusion

In this paper, a numerical method has been proposed to model the effect of fretting on surface damage and contact solution. A three-dimensional contact solver with heterogeneous elastic damageable model is developed based on the Eshelby's equivalent inclusion method. Multiple cuboidal inclusions are surimposed on the half space solution as an enrichment technique. The model has been validated by performing a comparison with the the Hertzian contact solution. The model allow to simulate fretting cycles while taking into account the damage evolution of the surface and his influence on the contact solution. The following major conclusions have been reached :

- The proposed method permits to couple the contact problem, the presence of heterogeneous inclusions and a damage law. The algorithm is very robust and convergence can be easily reached even with high level of dam-

age. Influence of the computation discretization and enrichment size have been performed to proof the accuracy of the simulations.

- Contact pressure and shear distributions have been investigated along with the damage evolution for both gross slip and partial slip regimes.

- The results obtained with our model are in good agreement with the surface damage phenomenon caused by fretting. The proposed method reproduce accurately some classical results of the literature [7]. The model proposed in Ghosh et al. [18] have been implemented in the semi-analytical solver along with the jump in cycle algorithm and a good agreement have been found between the two models.

- The enrichment technique allows to simulate fretting contact on coated material. The influence of these coatings on the damage localization in the material has been explicited. In agreement with the literature [64, 65], it is found again that hard coatings are protecting the surface from fretting damage.

The present work is made on the assumption of linear elasticity to keep the model simple and demonstrate its capability. To be more realistic, the present model could be improved by taking into account plasticity effects during the fretting cycles.

References

[1] O. Vingsbo, S. Soderberg, On fretting maps, Wear 126 (2) (1988) 131–147.

[2] R. D. Mindlin, Compliance of elastic bodies, Journal of Applied Mechanics 71 (1949) 259–268.

[3] D. Scott, Surface studies in the investigation of failure mechanisms, Proceedings of the Institution of Mechanical Engineers, Conference Proceedings 182(11) (1967) 56–64.

Nomenclature

Letters

a^*	contact radius
B^*_{ijkl}	influence coefficients that relating the stress σ_{ij} at point (x_1^3, x_2, x_3) to the constant eigenstrain at the point (x_1^k, x_2^k, x_3^k)
C^M_{ijkl}, C^I_{ijkl}	elastic constants of the matrix and the inhomogeneity
E^I	Young's modulus of the inhomogeneity
H	Hardness of the material
S_{ut}	Ultimate tensile stress
h	distance between the two surfaces of the contacting bodies
I_{ijkl}	the fourth-order identity tensor
K^n	coefficients in the normal displacement at the contact surface due to the contact pressure
M_{ij}	influence coefficients relating the stress σ_{ij} at the point (x_1, x_2, x_3) to the normal traction σ^n within a discretized area centered at $(x_1^k, x_2^k, 0)$
n_1, n_2, n_3	grid sizes in the half-space along the Cartesian directions x_1, x_2, x_3, respectively
W	normal applied load
P_0	maximum Hertzian pressure
P	contact pressure distribution
R	indenter radius
S_{ijkl}	components of the Eshelby's tensor
u_i^0	displacements corresponding to the infinite applied strain ε_{ij}^0
u_i	disturbed contribution of the displacements
$x^I = (x^I, y^I, z^I)$	Cartesian coordinates of the inclusion center
D	damage variable
δD	damage increment
E	undamaged Young's of the inhomogeneity
N Number of cycles	
$\tilde{E}$	effective Young's modulus
z_c	thickness of the coating.
N_i	Number of inclusions in the enrichment along direction i.

Greek letters

$\tilde{\sigma}$	effective stress

[4] N. Suh, The delamination theory of wear, Wear 25 (1) (1973) 111–124.

[5] U. Bryggman, S. Soderberg, Contact conditions and surface degradation mechanisms in low amplitude fretting, Wear 125 (1-2) (1988) 39–52.

[6] Z. R. Zhou, M. Vincent, Effect of external loading on wear maps of aluminium alloys, Wear 162-164 (1993) 619–623.

[7] L. Vincent, Y. Berthier, M. Godet, Testing methods in fretting fatigue : a critical appraisal, ASTM STP 1159 (1992) 33–48.

[8] P. Blanchard, C. Colombie, V. Pellerin, S. Fayeulle, L. Vincent, Material effects in fretting wear : Application to iron, titanium and aluminium alloys, Mettalurgical Transactions A 22 (7) (1991) 1535–1544.

[9] J. Lemaitre, A course on damage mechanics, Springer-Verlag, 1992.

[10] B. Bhattacharya, B. Ellingwood, Continuum damage mechanics analysis of fatigue crack initiation, International Journal of Fatigue 20 (9) (1998) 631–639.

[11] A. Beheshti, M. Khonsari, A thermodynamic approach for prediction of wear coefficient under unlubricated sliding condition, Tribology Letters 38 (3) (2010) 347–354.

[12] P. Ireman, A. Klarbring, N. Stromberg, A model of damage coupled to wear, International Journal of Solids and Structures 40(12) (2003) 2957–2974.

[13] N. A. Bhatti, K. Pereira, M. A. Wahab, A continuum damage mechanics approach for fretting fatigue under out of phase loading, Tribology International 117 (2018) 39 – 51.

[14] A. Beheshti, M. Khonsari, On the prediction of fatigue crack initiation in rolling/sliding contacts with provisition for loading sequence effect, Tribology International 44 (2011) 1620–1628.

[15] N. Raje, F. Sadeghi, R. G. Rateick, A statistical damage mechanics model for subsurface initiatied spalling in rolling contacts, Journal of Tribology 130(4) (2008) 042201.

[16] N. Raje, T. Slack, F. Sadeghi, A discrete damage mechanics model for high cycle fatigue in polycristalline materials subject to rolling contact., International Journal of Fatigue 31(2) (2009) 685–697.

[17] A. Warhadpande, B. Jalalahmadi, T. Slack, F. Sadeghi, A new finite element fatigue modeling approach for life scatter in tensile steel specimens, International Journal of Fatigue 32(4) (2010) 685–697.

[18] A. Ghosh, B. Leonard, F. Sadeghi, A stress based damage mechanics model to simulate fretting wear of hertzian line contact in partial slip, Wear 307 (2013) 87–99.

[19] A. Ghosh, W. Wang, F. Sadeghi, An elastic-plastic investigation of third body effects on fretting contact in partial slip, International Journal of Solids and Structures 81 (2016) 95–109.

[20] F. Shen, H. Weiping, M. Qingchun, A damage mechanics approach to fretting fatigue life prediction with consideration of elastic-plastic damage model and wear, Tribology International 82 (2015) 176–190.

[21] D. Kumar, R. Biswas, L. H. Poh, M. A. Wahab, Fretting fatigue stress analysis in heterogeneous material using direct numerical simulations in solid mechanics, Tribology International 109 (2017) 124 – 132.

[22] T. Dick, G. Cailletaud, Fretting modelling with a crystal plasticity model of ti6al4v, Computational Materials Science 38 (1) (2006) 113–125.

[23] S. Fouvry, Liskiewicz, C. Paulin, A global-local wear approach to quantify the contact endurance under reciprocating fretting sliding conditions, Wear 263 (1) (2007) 518–531.

[24] C. Paulin, S. Fouvry, C. Meunier, Finite element modelling of fretting wear surface evolution : application to a ti-6a1-4v contact, Wear 264(1-2) (2008) 26–36.

[25] T. Yue, M. Abdel Wahab, Finite element analysis of fretting wear under variable coefficient of friction and different contact regimes, Tribology International 107 (2017) 274–282.

[26] L. Gallego, D. Nelias, C. Jacq, A comprehensive method to predict wear and to define the optimum geometry of fretting surfaces, ASME Journal of Tribology 128 (2006) 476–485.

[27] L. Gallego, D. Nelias, Modeling of fretting wear under gross slip and partial slip conditions, Journal of Tribology 129 (3) (2007) 528–535.

[28] L. Gallego, D. Nelias, S. Deyber, A fast and efficient contact algorithm for fretting problems applied to fretting modes i, ii and iii, Wear 268 (1) (2010) 208–222.

[29] V. Done, D. Kesavan, R. Murali Krishna, T. Chaise, D. Nelias, Semi analytical fretting wear simulation including wear debris, Tribology International 109 (2017) 1–9.

[30] C. Jacq, D. Nelias, G. Lormand, D. Girodin, Development of a three-dimensional semi-analytical elastic-plastic contact code, Journal of Tribology 124(4) (2002) 653–667.

[31] V. Boucly, D. Nelias, S. Liu, Q. Wang, L. Keer, Contact analyses for bodies with frictional heating and plastic behavior, Journal of tribology 127 (2005) 355–364.

[32] F. Wang, L. Keer, Numerical simulation for three-dimensional elastic-plastic conact with hardening behavior, ASME Journal of Tribology 127(3) (2005) 494–502.

[33] D. Nelias, E. Antaluca, V. Boucly, Rolling of an elastic ellipsoid upon an elastic-plastic flat, ASME Journal of Tribology 129 (4) (2007) 791–800.

[34] T. Chaise, D. Nelias, Contact pressure and residual strain in 3d elasto-plastic rolling contact for a circular or elliptical point contact, Journal of Tribology 133 (4) (2011) 041402.

[35] T. Chaise, J. Li, D. Nelias, R. Kubler, S. Taheri, G. Douchet, V. Robin, P. Gilles, Modelling of multiple impacts for the prediction of distortions and residual stresses induced by ultrasonic shot peening (usp), Journal of Materials Processing Technology 212 (2012) 2080–2090.

[36] T. Chaise, D. Nelias, F. Sadeghi, On the effect of isotropic hardening on the coeffcient of restitution for single or repeated impacts using a semi-analytical method, Tribology Transactions 54 (5) (2011) 714–722.

[37] W. W. Chen, Q. J. Wang, F. Wang, L. M. Keer, J. Ciao, Three-dimensional repeated elasto-plastic point contacts, rolling, and sliding, Journal od Applied Mechanics 75 (2008) 021021.

[38] K. Zhou, W. Chen, L. Keer, Q. Wang, A fast method for solving three-dimensional arbitrarily shaped inclusions in a half space, Computer Methods in Applied Mechanics and Engineering 198 (9-12) (2009) 885–892.

[39] K. Zhou, W. Chen, L. Keer, X. Ai, K. Sawamiphakdi, P. Glaws, Q.Wang, Multiple 3d inhomogeneous inclusions in a half space under contact loading, Mechanics of Materials 43 (2011) 444–457.

[40] K. Zhou, L. M. Keer, Q. J. Wang, Semi-analytic solution for multiple interacting three-dimensional inhomogeneous inclusions of arbitrary shape in an infinite space, International Journal for Numerical Methods in Engineering 87 (2011) 617–638.

[41] K. Zhou, L. M. Keer, Q. J. Wang, X. Ai, K. Sawamiphakdi, P. Glaws, Interaction of multiple inhomogeneous inclusions beneath surface, Comput. Methods Appl. Mech. Engrg. 217-220 (2012) 25–33.

[42] J. Leroux, B. Fulleringer, D. Nelias, Contact analysis in presence of spherical inhomogeneities within a half-space, International Journal of Solids and Structures 47 (2010) 3034–3049.

[43] J. Leroux, D. Nelias, Stick-slip analysis of a circular point contact between a rigid sphere and a flat unidirectional composite with cylindrical fibers, International Journal of Solids and Structures 48 (2011) 3510–3520.

[44] K. Koumi, L. Zhao, J. Leroux, T. Chaise, D. Nelias, Contact analysis in the presence of an ellipsoidal inhomogeneity within a half space, International Journal of Solids and Structures 51 (2014) 1390–1402.

[45] K. Koumi, D. Nelias, T. Chaise, A. Duval, Modeling of the contact between a rigid indenter and a heteregeneous viscoelastic material, Mechanics of Materials 77 (2014) 28–42.

[46] K. Koumi, T. Chaise, D. Nelias, Rolling contact of a rigid sphere/sliding of a spherical indenter upon a viscoelastic half-space containing an ellipsoidal inhomogeneity, Journal of the Mechanics and Physics of Solids 80 (2015) 1–25.

[47] K. V. Amuzuga, T. Chaise, A. Duval, D. Nelias, Fully coupled resolution of heterogeneous elastic-plastic contact problem, Journal of Tribology 138 (2016) 021403–1.

[48] C. Bagault, D. Nelias, M.-C. Baietto, Contact analyses for anisotropic half space : Effect of the anisotropy on the pressure distribution and contact area, Journal of tribology 134 (3) (2012) 031401 (8 pages).

[49] C. Bagault, D. Nelias, M.-C. Baietto, T. Ovaert, Contact analyses for anisotropic half-space coated with an anisotropic layer : Effect of the anisotropy on the pressure distribution and contact area, International Journal of Solids and Structures 50 (5) (2013) 743–754.

[50] I. Polonsky, L. Keer, A numerical method for solving rough contact problems based on the multi-level multi-summation and conjugate gradient techniques, Wear 231 (2) (1999) 206–219.

[51] Z. Moschovidis, T. Mura, Two-ellipsoidal inhomogeneities by the equivalent inclusion method, Journal of Applied Mechanics 42 (1975) 847–852.

[52] Y. Chiu, On the stress field and surface deformation in a half space with a cuboidal zone in which initial strains are uniform, Journal of Applied Mechanics 45 (1978) 302–306.

[53] T. Mura, Micromechanics of Defects in Solids, 2nd Edition, Kluwer Academic Publishers, 1987.

[54] S. Liu, Q. Wang, G. Liu, A versatile method of discrete convolution and fft (dc-fft) for contact analyses, Wear 243 (1-2) (2000) 101–111.

[55] A. Love, A Treatise on the Mathematical Theory of Elasticity, 4th Edition, Cambridge University Press, 1952.

[56] K. Johnson, Contact Mechanics, Cambridge University Press, 1985.

[57] L. M. Kachanov, Time of the rupture process under creep conditions, Izvestia Akademii Nauk SSSR, Otdelenie tekhnicheskich nauk 8 (1958) 26–31.

[58] Y. Rabotnov, Creep problemes in structural members, Amesterdam: North Holland.

[59] J. Lemaitre, A continuous damage mechanics model for ductile fracture, Journal of Engineering Materials and Technology 107 (1985) 83–89.

[60] J. Mazars, G. Pijaudier-Cabot, Continuum damage theroy - application to concrete, Journal of Engineering Mechanics 115 (2) (1989) 345–365.

[61] S. Fouvry, P. Du, P. Perruchaut, A quantitative approach of ti-6al-4v fretting damage : friction, wear and crack nucleation, Wear 257(9-10) (2004) 916–929.

[62] J.-L. Chaboche, P. Lesne, A non-linear continuous fatigue damage model, Fatigue and Fracture of Engineering Materials and Structures 11 (1) (1988) 1–17.

[63] T. Slack, F. Sadeghi, Explicit finite element modeling of subsurface initated spalling in rolling contacts, Tribology International 43 (9) (2010) 1693–1702.

[64] J. Beard, The rational selection of palliatives for avoidance of fretting, Proceedings of the Institution of Mechanical Engineers International Conference: Tribology - Friction, Lubrication and Wear Fifty Years On (1987) 311–319.

[65] S. Fouvry, P. Kapsa, H. Zahouani, L. Vincent, Wear analysis in fretting of hard coatings through a dissipated energy concept, Wear 203-204 (1997) 393–403.

[66] S. Gordelier, T. Chivers, A literature review of palliatives for fretting fatigue, Wear 56 (1979) 177–190.

Appendix A. Stress in a half-space due to a concentrated unit normal force at the surface origin(F_{ij})

$$F_{11}(x,y,z) = \frac{1}{2\pi}\left[\frac{1-2\nu}{r^2}(1-\frac{z}{\rho})\frac{x^2-y^2}{r^2} + \frac{zy^2}{\rho^3} - \frac{3zx^2}{\rho^5}\right],$$

$$F_{22}(x,y,z) = F_{11}(y,x,z),$$

$$F_{33}((x,y,z)) = -\frac{3}{2\pi}\frac{z^3}{\rho^5},$$

$$F_{12}((x,y,z)) = \frac{1}{2\pi}\left[\frac{1-2\nu}{r^2}(1-\frac{z}{\rho})\frac{xy}{r^2} + \frac{zyx}{\rho^3} - \frac{3zyx}{\rho^5}\right],$$

$$F_{13}((x,y,z)) = -\frac{3}{2\pi}\frac{xz^2}{\rho^5},$$

$$F_{23}((x,y,z)) = F_{12}(y,x,z),$$

where

$$r^2 = x^2 + y^2, \quad \rho = \sqrt{x^2+y^2+z^2},$$

with ν, the Poisson's ratio of the isotropic half-space.

Appendix B. Stresses in a half-space subject to normal pressure (M_{ij})

An isotropic half-space is submitted a uniform normal pressure σ^n in a discretized surface area of $2\Delta x \times 2\Delta y$ at the center point $P(x', y', 0)$. The stress at an observation point $Q(x, y, z)$ is given in [38] and [56]:

$$\begin{aligned}\sigma_{ij}(x,y,z) &= M_{ij}(x-x', y-y', z)\sigma^n(x,y)\\ \sigma_{ij}(x,y,z) &= \frac{\sigma^n}{2\pi}[h_{ij}(\xi_1+\Delta x, \xi_2+\Delta y, \xi_3) - h_{ij}(\xi_1+\Delta x, \xi_2-\Delta y, \xi_3)\\ &\quad + h_{ij}(\xi_1-\Delta x, \xi_2-\Delta y, \xi_3) - h_{ij}(\xi_1-\Delta x, \xi_2+\Delta y, \xi_3)]\end{aligned}$$

where

$$\xi_1 = x - x'.\xi_2 = y - y'.\xi_3 = z - z'.$$

The functions $h_{ij}()$ in Eq.(B1) are defined by

$$h_{11}((x,y,z) = 2\nu\tan^{-1}\frac{y^2+z^2-\rho y}{xz} + 2(1-\nu)\tan^{-1}\frac{\rho - y + z}{x} + \frac{xyz}{\rho(x^2+z^2)},$$

$$h_{22}((x,y,z) = h_{11}(y,x,z),$$

$$h_{33}((x,y,z) = \tan^{-1}\frac{y^2+z^2-\rho y}{xz} - \frac{xyz}{\rho}\left(\frac{1}{x^2+z^2} + \frac{1}{y^2+z^2}\right),$$

$$h_{12}((x,y,z) = -\frac{z}{\rho} - (1-2\nu)\log(\rho+z),$$

$$h_{13}((x,y,z) = -\frac{yz^2}{\rho(x^3+z^2)},$$

$$h_{23}((x,y,z) = h_{13}(y,x,z),$$

where

$$rho = \sqrt{x^2+y^2+z^2}.$$

Appendix C. Normal displacement at the surface subject to normal pressure (K^n)

The contact between a sphere and an elastic half-space having respectively elastic constants (E_1, ν_1) and (E_2, ν_2), where the surface $z = 0$ is discretized into rectangular surface area of $2\Delta_1 \times 2\Delta_2$, is now considered. The initial contact point coincides with the origin of the Cartesian coordinate system $((x, y, z)$. The relationship between the normal displacement at an observation point $P(\xi_1, \xi_2, 0)$ and the pressure field at the center $Q(\xi_1', \xi_2', 0)$ is built using the function K^n.

$$K^n(c_1, c_2) = \left[\frac{1-\nu_1^2}{\pi E_1} + \frac{1-\nu_2^2}{\pi E_2}\right] \sum_{p=1}^{4} K_p^n(c_1, c_2),$$

$$K_1^n(c_1, c_2) = (c_1 + \Delta_1) \log\left(\frac{(c_2 + \Delta_2) + \sqrt{(c_2 + \Delta_2)^2 + (c_1 + \Delta_1)^2}}{(c_2 - \Delta_2) + \sqrt{(c_2 - \Delta_2)^2 + (c_1 + \Delta_1)^2}}\right),$$

$$K_2^n(c_1, c_2) = (c_2 + \Delta_2) \log\left(\frac{(c_1 + \Delta_1) + \sqrt{(c_2 + \Delta_2)^2 + (c_1 + \Delta_1)^2}}{(c_1 - \Delta_1) + \sqrt{(c_2 + \Delta_2)^2 + (c_1 - \Delta_1)^2}}\right),$$

$$K_3^n(c_1, c_2) = (c_1 - \Delta_1) \log\left(\frac{(c_2 - \Delta_2) + \sqrt{(c_2 - \Delta_2)^2 + (c_1 - \Delta_1)^2}}{(c_2 + \Delta_2) + \sqrt{(c_2 + \Delta_2)^2 + (c_1 - \Delta_1)^2}}\right),$$

$$K_4^n(c_1, c_2) = (c_2 - \Delta_2) \log\left(\frac{(c_1 - \Delta_1) + \sqrt{(c_2 - \Delta_2)^2 + (c_1 - \Delta_1)^2}}{(c_1 + \Delta_1) + \sqrt{(c_2 - \Delta_2)^2 + (c_1 + \Delta_1)^2}}\right),$$

where

$$c_1 = \xi_1 - \xi_1' \quad \text{and} \quad c_2 = \xi_2 - \xi_2'$$